RSC Advances

ROYAL SOCIETY OF CHEMISTRY

www.rsc.org/advances

Journal Name

RSCPublishing

ARTICLE

Facile synthesis of hierarchical MnO_2 sub-microspheres composed of nanosheets and its application for supercapacitor

Lifang Lian, Jie Yang, Peixun Xiong, Weifeng Zhang and Mingdeng Wei *

Cite this: DOI: 10.1039/x0xx00000x

Received 00th January 2012,
Accepted 00th January 2012

DOI: 10.1039/x0xx00000x

www.rsc.org/

Hierarchical MnO_2 sub-microspheres were fabricated by using a simple, green and efficient low-temperature route. These sub-microspheres were formed via the aggregation of ultrathin nanosheets with a thickness of 2-4 nm. An electrode made of hierarchical MnO_2 sub-microspheres exhibited a specific capacitance of 120 F g^{-1} at a current density of 0.167 A g^{-1}. For an asymmetric AC//MnO_2 supercapacitor, it exhibited a superior electrochemical stability in 1 M Na_2SO_4 aqueous solution with a 88% retention of the initial specific capacitance after 1000 cycles, and the Coulombic efficiency was above 97%, indicating good charge-discharge reversibility and electrochemical stability.

Introduction

Supercapacitor, due to its high power density, fast charge-discharge ability and long cycling life, has been considered as a complement for batteries, or even can replace batteries in applications where high power delivery is needed.[1-4] Supercapacitor could be classified into two categories. One is the electrical double layer capacitors that store charge electrostatically using reversible absorption of electrolyte ions onto active materials; the other is the pseudocapacitors that depend on the reversible redox reaction at the surface of active materials.[3, 5] To date, the most widely used electrode materials in supercapacitors are carbonaceous materials (such as carbon nanotube,[6] carbon nanofiber[7] and grapheme[8] etc.), metal oxides (such as RuO_2,[9] V_2O_5[10] and MnO_2[15-19] etc.), and conducting polymers.[11] Among them, manganese oxides, characterized by high theoretical specific capacitance, nontoxicity, abundance, low-cost and environmental compatibility, have attracted much attention as a promising candidate for supercapacitor.[2,12]

Nanostructurization is one of major strategies in the development of high-performance manganese oxide-based electrodes for supercapacitor.[13] It is well known that the nanomaterials synthesized with controlled sizes, shapes, crystal phases, dimensions and compositions make it possible to tune material parameters for optimizing performance in supercapacitor. Moreover, nanoscale dimension may tolerate more distortion and strain caused by the intercalation/deintercalation of the ions, leading to long-term stability.[14] Therefore, many efforts have been devoted into the synthesis of MnO_2 with different morphologies, sizes, nanostructures and properties through various methods, such as hydrothermal reaction,[15] sol-gel method,[16] template method,[17] electro-deposition method,[18] precipitation method,[19] etc. In general, these methods usually need some rigorous reaction conditions including high temperature, high pressure, long reaction time, complex and costly procedures, which are not versatile or environmental friendly. Therefore, the development of a facile and green route for synthesizing MnO_2 is still of great significance.

In the present work, a simple and efficient reduction route was successfully developed for fabricating hierarchical sub-microspheres of MnO_2 on a large scale. Furthermore, hierarchical MnO_2 sub-microspheres were used as an electrode for supercapacitor and exhibited a good electrochemical performance.

Experimental

Hierarchical MnO_2 sub-microspheres were synthesized via a facile reduction route. In a typical synthesis, 1.0 g of SDBS and 0.632 g of $KMnO_4$ were added to 50 mL of 0.2 M sulfuric acid solution with stirring, and then was kept at 50 °C for 4 h in a water bath. Finally, the precipitate was filtered and washed

several times with deionized water and then dried at 70 °C for 12 h.

XRD patterns were recorded on PANalytical X'Pert spectrometer using the Co-Ka radiation and the data were changed to Cu-Ka data. X-ray photoelectron spectroscopy (XPS) measurements (ESCALAB 250) were performed to analyze the surface species and their chemical states. Scanning electron microscopy (SEM) and transmission electron microscopy (TEM) were taken on a Hitachi S4800 instrument and a FEI F20 S-TWIN instrument, respectively.

Electrochemical properties of the samples were evaluated in a standard three electrode test pool (Hangzhou Saiao Electrochemistry Technology Co., Ltd). For the working electrode, a mixture containing of 70 wt. % active material, 20 wt. % acetylene black, and 10 wt. % PTFE binder was well mixed. Then the mixture was pressed with several drops of isopropyl alcohol solvent to form a thin sheet. The sheet was rolled to get approximate thickness of 100 μm and then pressed onto the nickel foam. The mass loading of the activated material was about 5 mg cm^{-2}. Pt electrode and saturated calomel electrode (SCE) were used as the counter and reference electrodes, respectively. All electrochemical measurements were carried out in 1 M Na_2SO_4 aqueous electrolyte using an IM6 Electrochemical Workstation (Zahner). For the fabrication of the asymmetric supercapacitor, active carbon (AC) electrodes were first prepared by the way same with MnO_2 electrodes. Then the MnO_2 electrode was used as positive electrode and AC electrode was used as negative electrode, respectively. The mass ratio of positive electrode/negative electrode was 1:2 (based on charge balance theory and their respectively specific capacitance). The charge-discharge tests for the asymmetric supercapacitors were performed on the Land automatic batteries tester (Land CT 2001A, Wuhan, China). The discharge specific capacitance was calculated according to the following equation:

$$C_{sp} = \frac{I \times \Delta t}{m \times \Delta U}$$

where I (A) is the applied current, Δt (s) is the discharge time, ΔU (V) is the tested potential range, and m (g) is the mass of tested active material within the electrodes.

Results and discussion

Fig. 1a shows the XRD pattern of MnO_2 and clearly shows two characteristic peaks at 37.1° and 66.3°, indicating the amorphous nature of MnO_2.[20] Fig. 1b reveals that the synthesized MnO_2 exhibited a spherical structure with a diameter of 300-500 nm. A SEM image in Fig. 1c demonstrates that the spherical structure was formed by the aggregation of nanosheets. A TEM image focused on a single sphere is shown in Fig. 1d and further confirmed that the spherical structure was formed via the aggregation of nanosheets with a typical thickness of 2-4 nm. The selective area electronic diffraction (SAED) (Fig. 1d inset) shows that the synthesized MnO_2 was amorphous,[21] which was consistent with XRD.

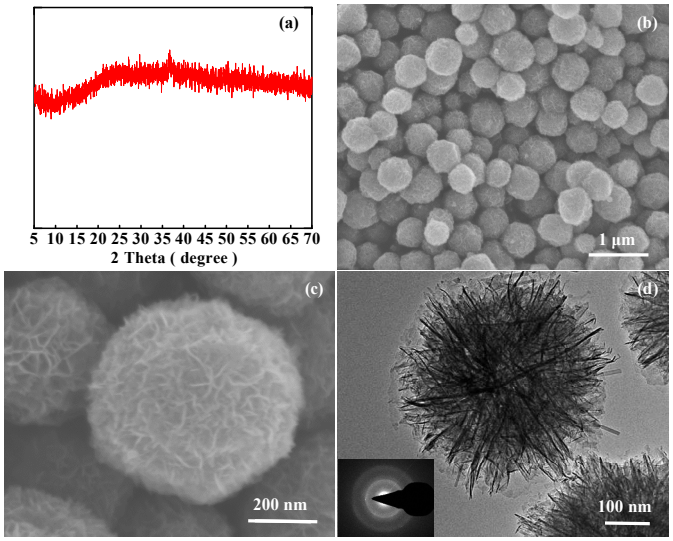

Fig. 1 (a) XRD pattern of MnO_2, (b-c) SEM and (d) TEM images of the MnO_2 sample. The inset in (d) is the SAED pattern of the MnO_2 sample.

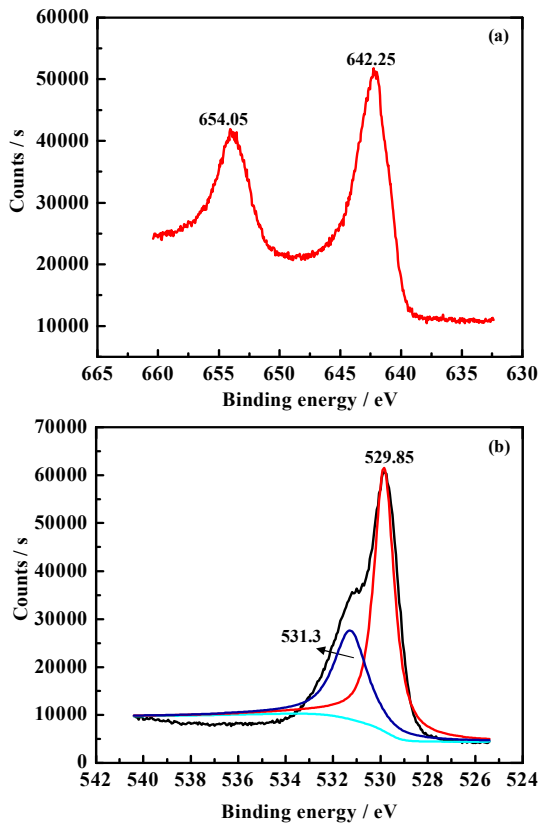

Fig. 2 XPS spectra of MnO_2: (a) Mn 2p and (b) O 1s.

The XPS spectrum was used to further determine the oxidation state of the obtained MnO_2. As depicted in Fig. 2a, it clearly reveals that the binding energy peaks of Mn $2p_{3/2}$ and

Mn $2p_{1/2}$ centered at 642.25 and 654.05 eV, respectively, which were in good agreement with the reported date for MnO_2.[12] The average oxidation state of Mn was around 3.55 based on the analysis of O 1s spectrum (Fig. 2b).[12, 20, 22]

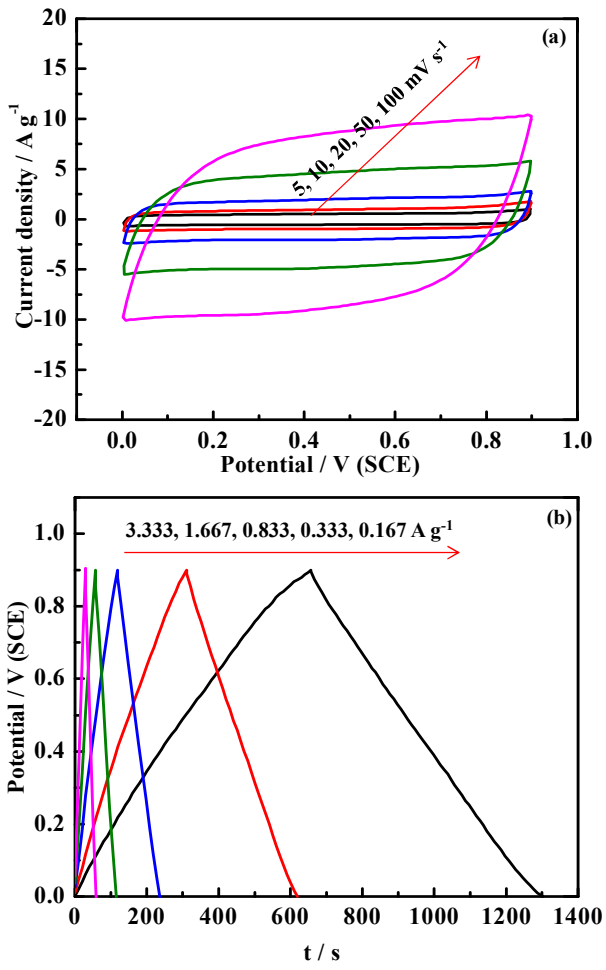

Fig. 3 (a) CV curves at different scan rates and (b) charge-discharge profiles at different current densities of MnO_2 electrodes.

Fig. 3a shows the CV curves of MnO_2 sub-microspheres at different scan rates ranging from 5 to 100 mV s^{-1} with a potential window of 0 to 0.9 V. It clearly reveals an approximately rectangular shape which can keep a nearly rectangular at scan rate even as high as 100 mV s^{-1}, indicating a typical pseudocapacitive behavior of MnO_2.[22, 23] In addition, a pair of light redox peaks could be observed at low scan rate of 10 mV s^{-1} (Fig. S1), revealing a fast and reversible Fradic reaction between alkali cations (Na^+) and ultrathin MnO_2 nanosheets. [22-24] Fig. 3b shows the galvanostatic charge-discharge curves of MnO_2 sub-microspheres at different current densities and the specific capacitances were 120 and 107 F g^{-1} at 0.167 and 3.333 A g^{-1}, respectively. When the current density was increased from 0.167 to 3.333 A g^{-1}, 89.16% of the initial capacitance could be retained, demonstrating a good rate capability.

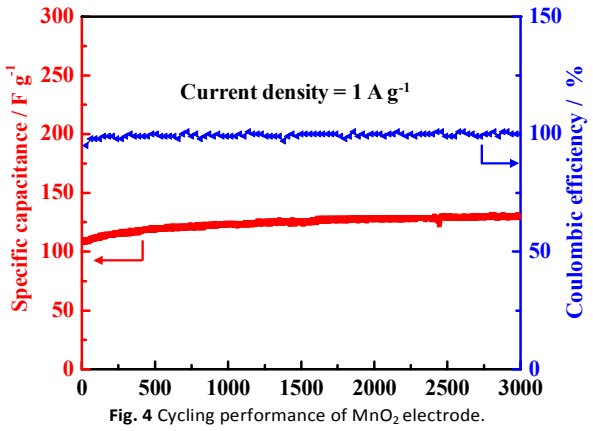

Fig. 4 Cycling performance of MnO_2 electrode.

Fig. 4 shows the cycling performance of MnO_2 sub-microspheres at a current density of 1 A g^{-1}. The specific capacitance increased slightly over the whole 3000 cycles which was similar to some reports on manganese oxide electrode materials.[25,26] The increase of the specific capacitance may be attributed to the activation effect of electrochemical cycling.[25] This demonstrated that the electrode of MnO_2 sub-microspheres had a good electrochemical stability.

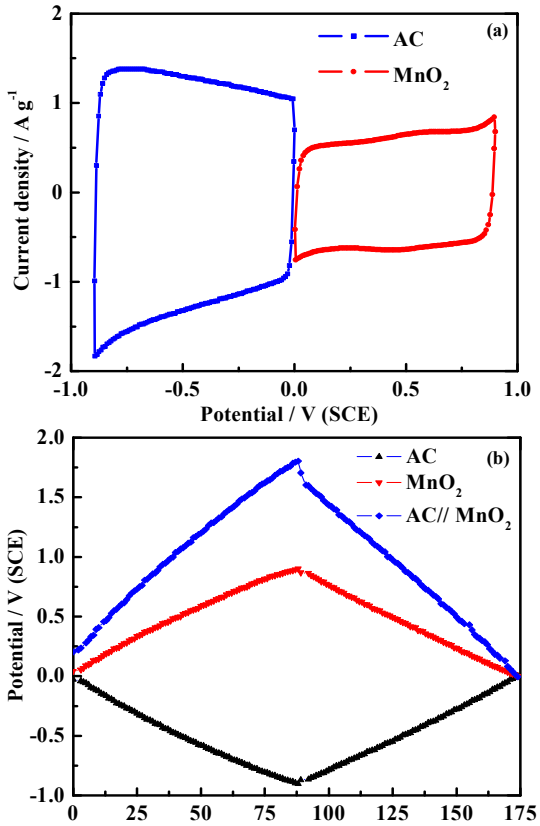

Fig. 5 (a) CV curves of the MnO_2 and AC electrodes, (b) charge-discharge profiles of the individual electrode (MnO_2 and AC), along with the voltage profile of AC//MnO_2 asymmetric supercapacitor.

To further investigate the electrochemical performance of MnO_2 sub-microspheres, an asymmetric supercapacitor based

on MnO_2 and AC was fabricated. Before the test of a full cell, CV measurements were performed on the two electrodes to estimate the stable potential windows of MnO_2 and AC. The MnO_2 electrode was measured within a potential window of 0 to 0.9 V, while AC electrode was measured within a potential window of -0.9 to 0 V at a scan rate of 10 mV s^{-1}, as shown in Fig. 5a. Both MnO_2 and AC electrodes exhibited a nearly ideal rectangular shape at their corresponding potential windows, demonstrating their stable electrochemical performance, therefore, it is expected that the operation voltage can be extended to 1.8 V in 1 M Na_2SO_4 aqueous solution. Fig. 5b shows the charge-discharge profiles of the individual electrodes *vs*. SEC reference electrode and the voltage profile of the asymmetric AC//MnO_2 supercapacitor in 1 M Na_2SO_4 aqueous solution. It can also be observed from Fig. 5b that the AC//MnO_2 asymmetric supercapacitor displayed a slope voltage profile from 0 to 1.8 V, which was resulted from the potential difference between the positive electrode of MnO_2 and the negative electrode of AC.

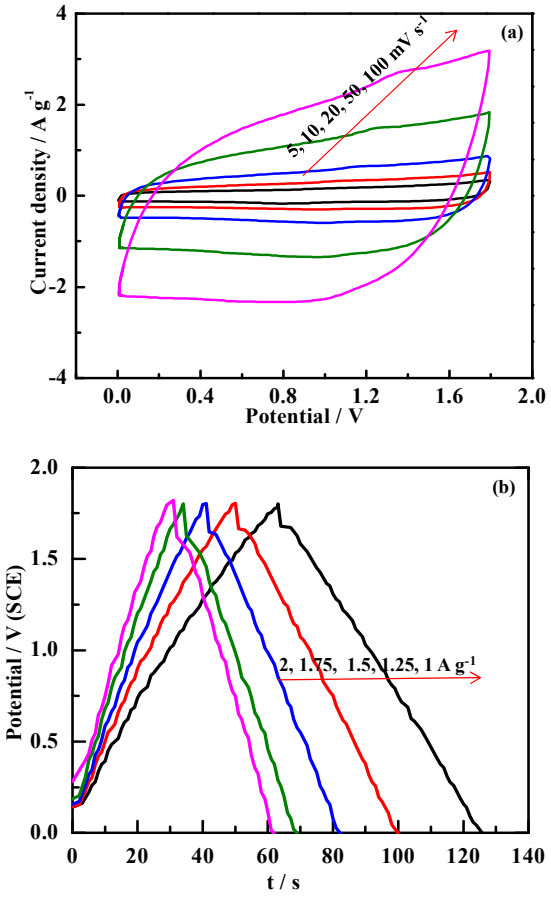

Fig. 6 (a) CV curves at different scan rates and (b) Charge-discharge profiles at different current densities of AC//MnO_2 asymmetric supercapacitor.

Fig. 6a shows the CV curves of an asymmetric AC//MnO_2 supercapacitor at different scan rates. It exhibits a good capacitive behavior with a nearly rectangular CV curves, indicating that the stable electrochemical window of the asymmetric supercapacitor can be extended to 1.8 V. Fig. 6b shows the galvanostatic charge-discharge profiles for an asymmetric AC//MnO_2 supercapacitor at different current densities. The specific capacitance at a current density of 1 A g^{-1} (based on the total mass of active materials on the two electrodes) was 34.4 F g^{-1}. When the current density was increased from 1 to 2 A g^{-1}, 96% of the initial capacitance can be retained, indicating a good rate capability. The supercapacitor delivered an energy density of 15.84 Wh kg^{-1} at a power density of 885 W kg^{-1}, and cab be maintained a value of 14.85 Wh kg^{-1} at a power density of 1725 W kg^{-1}, which were much higher than symmetrical supercapacitors reported in literatures such as MnO_2//MnO_2,[27] AC//AC,[28] and CNTs//CNTs.[29] This is also higher or comparable to those of other asymmetric supercapacitors such as PANI//MnO_2,[30] PPY//MnO_2,[30] PEDOT//MnO_2,[30] Fe3O4//MnO_2[31] and AC//MnO_2.[32, 33]

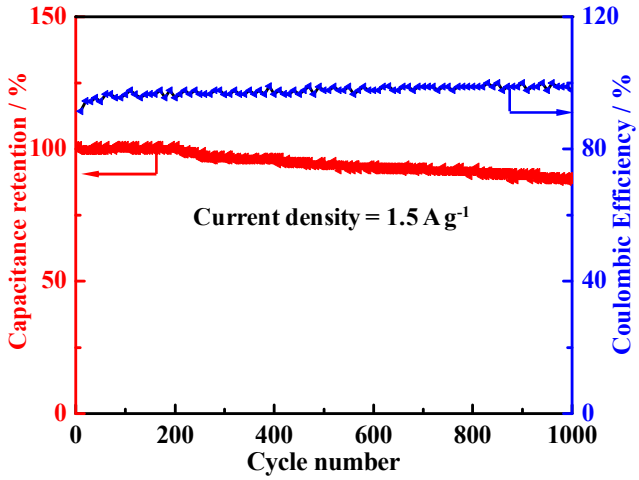

Fig. 7 Cycling performance of AC//MnO_2 asymmetric supercapacitor.

Fig. 7 shows the cycling performance for an asymmetric AC//MnO_2 supercapacitor at a current density of 1.5 A g^{-1} in 1 M Na_2SO_4 aqueous solution; this device exhibited a superior electrochemical stability with a 88% retention of the initial specific capacitance (34 F g^{-1}) after 1000 cycles. Such cycling performance was superior or at least comparable to those of other asymmetric supercapacitors, such as graphene//MnO_2/ grapheme,[34] AC//α-MnO_2·nH_2O[35] and AC//MnO_2.[36] The capacitance fading was attributed to the corrosion of the current collector arising from the presence of dissolved oxygen in the aqueous electrolyte[33] or matching problem.[37] The Coulombic efficiency of the asymmetric supercapacitor was above 97%, indicating good charge-discharge reversibility and electrochemical stability.[38]

As mentioned above, MnO_2 sub-microspheres used as the electrode in a three-electrode system or an asymmetric supercapacitor all exhibited a good supercapacitive performance, which may be attributed to the intrinsic characteristics of MnO_2 sub-microspheres. MnO_2 sub-microspheres with a hierarchically porous structure can permit facile diffusion of the electrolyte, and also enhance the contact

between the electrode surface and the electrolyte; while ultrathin nanosheets can shorten the transport distance of electrolytes and electrons during electrochemical cycling, leading to large capacitance, high rate capability and cycling stability.

Conclusions

In summary, a simple and effective route was developed for fabricating hieratical MnO_2 sub-microspheres. These sub-microspheres were formed via the aggregation of ultrathin nanosheets with a thickness of 2-4 nm. The electrochemical measurements indicated that hierarchical MnO_2 sub-microspheres exhibited large capacitance, high rate capability and long-term cycling stability. Thus, such a hierarchically porous nanostructure can serve as promising electrode materials for supercapacitors.

Acknowledgements

This work was financially supported by National Natural Science Foundation of China (NSFC 21173049; J1103303).

Notes and references

[a] Institute of Advance Energy Materials, Fuzhou University, Fuzhou, Fujian 350002, China
Tel./fax: +86-591-83753180; *E-mail address:* wei-mingdeng@fzu.edu.cn

1 G. P. Wang, L. Zhang and J. J. Zhang, *Chem. Soc. Rev.*, 2012, **41**, 797.
2 P. Y. Tang, Y. Q. Zhao, Y. M. Wang and C. L. Xu, *Nanoscale*, 2013, **5**, 8156.
3 P. Simon and Y. Gogotsi, *Nat. Mater.*, 2008, **7**, 845.
4 L. H. Bao, J. F. Zang and X. D. Li, *Nano Lett.*, 2011, **11**, 1215.
5 M. J. Zhi, C. C Xiang, J. T. Li, M. Li and N. Q. Wu, *Nanoscale*, 2013, **5**, 72.
6 P. X. Li, C. Y. Kong, Y. Y. Shang, E. Z. Shi, Y. T. Yu, W. Z. Qian, F. Wei, J. Q. Wei, K. L. Wang, H. W. Zhu, A. Y. Cao and D. H. Wu, *Nanoscale*, 2013, **5**, 8472.
7 L. F. Chen, Z. H. Huang, H. W. Liang, W. T. Yao, Z. Y. Yu and S. H. Yu, *Energy Environ. Sci.*, 2013, **6**, 3331.
8 U. N. Maiti, J. Lim, K. E. Lee, W. J. Lee, and S. O. Kim, *Adv. Mater.*, 2014, **26**, 615.
9 C. C. Hu, K. H. Chang, M. C. Lin and Y. T. Wu, *Nano Lett.*, 2006, **6**, 2690.
10 J. Yang, T. B. Lan, J. D. Liu, Y. F. Song, M. D. Wei, *Electrochim. Acta*, 2013, **105**, 489.
11 L. Z. Fan and J. Maier, *Electrochem. Commun.*, 2006, **8**, 937.
12 Z. J. Su, C. Yang, C. J Xu, H. Y. Wu, Z. X. Zhang, T. Liu, C. Zhang, Q. H. Yang, B. H. Li and F. Y. Kang, *J. Mater. Chem. A.*, 2013, **1**, 12432.
13 W. F Wei, X. W. Cui, W. X. Chen and D. G. Ivey, *Chem. Soc. Rev.*, 2011, **40**, 1697.
14 S. Liu, S. H. Sun and X. Z. You, *Nanoscale*, 2014, **6**, 2037.
15 V. Subramanian, H. W. Zhu and B. Q. Wei, *J. Power Sources*, 2006, **159**, 361.
16 X. L. Wang, A. B. Yuan and Y. Q. Wang, *J. Power Sources*, 2007, **172**, 1007.
17 X. Y. Wang, X. Y. Wang, W. G. Huang, P. J. Sebastian and S. Gamboa, *J. Power Sources*, 2005, **140**, 211.
18 S. L. Chou, J. Z. Wang, S. Y. Chew, H. K. Liu and S. X. Dou, *Electrochem. Commun.*, 2008, **10**, 1724.
19 M. Toupin, T. Brousse and D. Belanger, *Chem. Mater.*, 2002, **14**, 3946.
20 Y. Hou, Y. W. Cheng, T. Hobson and J. Liu, *Nano Lett.*, 2010, **10**, 2727.
21 R. Liu and S. B. Lee, *J. Am. Chem. Soc.*, 2008, **130**, 2942.
22 M. Toupin, T. Brousse and D. Belanger, *Chem. Mater.*, 2004, **16**, 3184.
23 Q. T. Qu, P. Zhang, B. Wang, Y. H. Chen, S. Tian, Y. P. Wu, *J. Phys. Chem. C*, 2009, **113**, 14020.
24 Z. B. Lei, J. T. Zhang and X. S. Zhao, *J. Mater. Chem.*, 2012, **22**, 153.
25 H. Jiang, T. Sun, C. Z. Li and J. Ma, *J. Mater. Chem.*, 2012, **22**, 2751.
26 M. Toupin, T. Brousse, and D. Belanger, *Chem. Mater.*, 2002, **14**, 3946.
27 V. Khomenko, E. R. Piñero and F. Béguin, *J. Power Sources*, 2006, **153**, 183.
28 D. W. Wang, F. Li, M. Liu, G. Q. Lu and H. M. Cheng, *Angew. Chem.*, 2008, **120**, 379.
29 M. Kaempgen, C. K. Chan, J. Ma, Y. Cui and G. Gruner, *Nano Lett.*, 2009, **9**, 1872.
30 V. Khomenko, E. Raymundo-Pinero, E. Frackowiak and F. Beguin, *Appl. Phys. A*, 2006, **82**, 567.
31 T. Cottineau, M. Toupin, T. Delahaye, T. Brousse and D. Belanger, *Appl. Phys. A*, 2006, **82**, 599.
32 X. Zhang, P. Yu, H. T. Zhang, D. C. Zhang, X. Z. Sun and Y. W. Ma, *Electrochimica Acta*, 2013, **89**, 523.
33 T. Brousse, P. L. Taberna, O. Crosnier, R. Dugas, P. Guillemet, Y. Scudeller, Y. Zhou, F. Favier, D. Belanger and P. Simon, *J. Power Sources*, 2007, **173**, 633.
34 Z. S. Wu, W. C. Ren, D. W. Wang, F. Li, B. L. Liu and H. M. Cheng, *ACS Nano*, 2010, **4**, 5835.
35 M. S. Hong, S. H. Lee and S. W. Kim, *Electrochem. Solid State Lett.*, 2002, **5**, A227.
36 X. Zhang, X. Z Sun, H. T. Zhang, D. C. Zhang and Y. W. Ma, Mater. *Chem. Phys.*, 2012, **137**, 290.
37 J. L. Li and F. Gao, *J. Power Sources*, 2009, **194**, 1184.
38 J. Y. Tao, N. S. Liu, L. Y. Li, J. Su and Y. H. Gao, *Nanoscale*, 2014, **6**, 2922.